16. Noguchi Y, Wu J, Duncan R, et al (1998) Early phase tumor accumulation of macromolecules: a great difference in clearance rate between tumor and normal tissues. Jpn J Cancer Res 89:307-314

17. Seymour LW, Miyamoto Y, Maeda H, et al (1995) Influence of molecular weight on passive tumour accumulation of a soluble macromolecular drug carrier. Eur J Cancer 31A:766-770

18. Maeda H (2001) The enhanced permeability and retention (EPR) effect in tumor vasculature: the key role of tumor-selective macromolecular drug targeting. Adv Enzyme Regul 41:189-207

19. Fang J, Nakamura H, Maeda H (2011) The EPR effect: unique features of tumor blood vessels for drug delivery, factors involved, and limitations and augmentation of the effect. Adv Drug Deliv Rev 63:136-151

20. Maeda H, Fang J, Inutsuka T, Kitamoto Y (2003) Vascular permeability enhancement in solid tumor: various factors, mechanisms involved and its implications. Int Immunopharmacol 3:319-328

21. Wu J, Akaike T, Maeda H (1998) Modulation of enhanced vascular permeability in tumors by a bradykinin antagonist, a cyclooxygenase inhibitor, and a nitric oxide scavenger. Cancer Res 58:159-165

22. Maeda H, Bharate GY, Daruwalla J (2009) Polymeric drugs for efficient tumor-targeted drug delivery based on EPR-effect. Eur J Pharm Biopharm 71:409-419

23. Maeda H (2010) Tumor-selective delivery of macromolecular drugs via the EPR effect: background and future prospects. Bioconjug Chem 21:797-802

24. Maeda H (2012) Vascular permeability in cancer and infection as related to macromolecular drug delivery, with emphasis on the EPR effect for tumor-selective drug targeting. Proc Jpn Acad Ser B 88:53–71

25. Fang J, Qin H, Nakamura H, Tsukigawa K, Shin T, Maeda H (2012) Carbon monoxide, generated by heme oxygenase-1, mediates the enhanced permeability and retention effect in solid tumors. Cancer Sci 103:535-541

26. Konerding MA, Miodonski AJ, Lametschwandtner A (1995) Microvascular corrosion casting in the study of tumor vascularity: a review. Scanning Microsc 9:1233-1243; discussion 1243-1244

27. Hashizume H, Baluk P, Morikawa S, et al (2000) Openings between defective endothelial cells explain tumor vessel leakiness. Am J Pathol 156:1363-1380

28. Kimura NT, Taniguchi S, Aoki K, Baba T (1980) Selective localization and growth of *Bifidobacterium bifidum* in mouse tumors following intravenous administration. Cancer Res 40:2061-2068

29. Zhao M, Yang M, Li XM, et al (2005) Tumor-targeting bacterial therapy with amino acid auxotrophs of GFP-expressing *Salmonella typhimurium*. Proc Natl Acad Sci U S A 102:755-760

30. Hoffman RM (2009) Tumor-targeting amino acid auxotrophic *Salmonella typhimurium*. Amino Acids 37:509-521

31. Papillon J, Dargent M, Chassard JL (1963) [Ultra-fluid lipiodol lymphography in cancerology (apropos of 62 cases)]. J Radiol Electrol Med Nucl 44:397-406

32. Konno T, Maeda H, Iwai K, et al (1983) Effect of arterial administration of high-molecular-weight anticancer agent SMANCS with lipid lymphographic agent on hepatoma: a preliminary report. Eur J Cancer Clin Oncol 19:1053-1065

33. Konno T, Maeda H, Iwai K, et al (1984) Selective targeting of anti-cancer drug and simultaneous image enhancement in solid tumors by arterially administered lipid contrast medium. Cancer 54:2367-2374

34. Maki S, Konno T, Maeda H (1985) Image enhancement in computerized tomography for sensitive diagnosis of liver cancer and semiquantitation of tumor selective drug targeting with oily contrast medium. Cancer 56:751-757

35. Iwai K, Maeda H, Konno T (1984) Use of oily contrast medium for selective drug targeting to tumor: enhanced therapeutic effect and X-ray image. Cancer Res 44:2115-2121

36. Veronese FM, Pasut G (2005) PEGylation, successful approach to drug delivery. Drug Discov Today 10:1451-1458

37. Sahoo SK, Sawa T, Fang J, et al (2002) Pegylated zinc protoporphyrin: a water-soluble heme oxygenase inhibitor with tumor-targeting capacity. Bioconjug Chem 13:1031-1038

38. Ogino T, Inoue M, Ando Y, Awai M, Maeda H, Morino Y (1988) Chemical modification of superoxide dismutase. Extension of plasma half life of the enzyme through its reversible binding to the circulating albumin. Int J Pept Protein Res 32:153-159

39. Rutter DA, Wade HE (1971) The influence of the iso-electric point of L-asparaginase upon its persistence in the blood. Br J Exp Pathol 52:610-614

40. Kimura M, Matsumura Y, Konno T, Miyauchi Y, Maeda H (1990) Enzymatic removal of bilirubin toxicity by bilirubin oxidase in vitro and excretion of degradation products in vivo. Proc Soc Exp Biol Med 195:64-69

41. Fang J, Sawa T, Akaike T, Maeda H (2002) Tumor-targeted delivery of polyethylene glycol-conjugated D-amino acid oxidase for antitumor therapy via enzymatic generation of hydrogen peroxide. Cancer Res 62:3138-3143

42. Maeda H, Takeshita J, Kanamaru R (1979) A lipophilic derivative of neocarzinostatin. A polymer conjugation of an antitumor protein antibiotic. Int J Pept Protein Res 14:81-87

43. Kojima Y, Haruta A, Imai T, Otagiri M, Maeda H (1993) Conjugation of Cu,Zn-superoxide dismutase with succinylated gelatin: pharmacological activity and cell-lubricating function. Bioconjug Chem 4:490-498

44. Hirano T, Todoroki T, Kato S et al (1994) Synthesis of the conjugate of superoxide dismutase with the copolymer of divinylether and maleic anhydride retaining enzymatic activity. J Cont Release 28: 203-209

45. Maeda H (2001) SMANCS and polymer-conjugated macromolecular drugs: advantages in cancer chemotherapy. Adv Drug Deliv Rev 46:169-185

46. Maeda H, Matsumura Y (1989) Tumoritropic and lymphotropic principles of macromolecular drugs. Crit Rev Ther Drug Carrier Syst 6:193-210

47. Greish K, Fang J, Inutsuka T, Nagamitsu A, Maeda H (2003) Macromolecular therapeutics: advantages and prospects with special emphasis on solid tumour targeting. Clin Pharmacokinet 42:1089-1105

48. Zhang JS, Liu F, Huang L (2005) Implications of pharmacokinetic behavior of lipoplex for its inflammatory toxicity. Adv Drug Deliv Rev 57:689-698

49. Dash PR, Read ML, Barrett LB, Wolfert MA, Seymour LW (1999) Factors affecting blood clearance and in vivo distribution of polyelectrolyte complexes for gene delivery. Gene Ther 6:643-650

50. Kwoh DY, Coffin CC, Lollo CP, et al (1999) Stabilization of poly-L-lysine/DNA polyplexes for in vivo gene delivery to the liver. Biochim Biophys Acta 1444:171-190

51. He C, Hu Y, Yin L, Tang C Yin C (2010) Effects of particle size and surface charge on cellular uptake and biodistribution of polymeric nanoparticles. Biomaterials 31:3657-3666

52. Daruwalla J, Nikfarjam M, Greish K, et al (2010) In vitro and in vivo evaluation of tumor targeting styrene-maleic acid copolymer-pirarubicin micelles: survival improvement and inhibition of liver metastases. Cancer Sci 101:1866-1874

53. Li CJ, Miyamoto Y, Kojima Y, Maeda H (1993) Augmentation of tumour delivery of macromolecular drugs with reduced bone marrow delivery by elevating blood pressure. Br J Cancer 67:975-980

54. Nagamitsu A, Greish K, Maeda H (2009) Elevating blood pressure as a strategy to increase tumor-targeted delivery of macromolecular drug SMANCS: cases of advanced solid tumors. Jpn J Clin Oncol 39:756-766

55. Suzuki M, Hori K, Abe I, Saito S, Sato H (1981) A new approach to cancer chemotherapy: selective enhancement of tumor blood flow with angiotensin II. J Natl Cancer Inst 67:663-669

56. Suzuki M, Hori K, Abe I, et al (1984) Functional characterization of the microcirculation in tumors. Cancer Metastasis Rev 3: 115-126

57. Noguchi A, Takahashi T, Yamaguchi T, et al (1992) Enhanced tumor localization of monoclonal antibody by treatment with kininase II inhibitor and angiotensin II. Jpn J Cancer Res 83:240-243

58. Jain RK (1990) Physiological barriers to delivery of monoclonal antibodies and other macromolecules in tumors. Cancer Res 50:814s-819s

59. Hori K, Suzuki M, Tanda S (1991) Fluctuations in tumor blood flow under normotension and the effect of angiotensin II-induced hypertension. Cancer Sci 82:1309-1316

60. Matsumoto K, Yamamoto T, Kamata R, Maeda H (1984) Pathogenesis of serratial infection: activation of the Hageman factor-prekallikrein cascade by serratial protease. J Biochem 96:739-749

61. Kamata R, Yamamoto T, Matsumoto K, Maeda H (1985) A serratial protease causes vascular permeability reaction by activation of the Hageman factor-dependent pathway in guinea pigs. Infect Immun 48:747-753

62. Maeda H, Matsumura Y, Kato H (1988) Purification and identification of [hydroxyprolyl$_3$]bradykinin in ascitic fluid from a patient with gastric cancer. J Biol Chem 263:16051-16054

63. Matsumura Y, Maruo K, Kimura M, Yamamoto T, Konno T, Maeda H (1991) Kinin-generating cascade in advanced cancer patients and in vitro study. Jpn J Cancer Res 82:732-741

64. Matsumura Y, Kimura M, Yamamoto T, Maeda H (1988) Involvement of the kinin-generating cascade in enhanced vascular permeability in tumor tissue. Jpn J Cancer Res 79:1327-1334

65. Cohen RA, Adachi T (2006) Nitric-oxide-induced vasodilatation: regulation by physiologic S-glutathiolation and pathologic oxidation of the sarcoplasmic endoplasmic reticulum calcium ATPase. Trends Cardiovasc Med 16:109-114

66. Lincoln TM (1989) Cyclic GMP and mechanisms of vasodilation. Pharmacol Ther 41:479-502

67. Doi K, Akaike T, Horie H, et al (1996) Excessive production of nitric oxide in rat solid tumor and its implication in rapid tumor growth. Cancer 77:1598-1604

68. Maeda H (2010) Nitroglycerin enhances vascular blood flow and drug delivery in hypoxic tumor tissues: analogy between angina pectoris and solid tumors and enhancement of the EPR effect. J Control Release 142:296-298

69. Seki T, Fang J, Maeda H (2009) Enhanced delivery of macromolecular antitumor drugs to tumors by nitroglycerin application. Cancer Sci 100:2426-2430

70. Jordan BF, Misson P, Demeure R, Baudelet C, Beghein N, Gallez B (2000) Changes in tumor oxygenation/perfusion induced by the NO donor, isosorbide dinitrate, in comparison with carbogen: monitoring by EPR and MRI. Int J Radiat Oncol Biol Phys 48:565-570

71. Yasuda H, Nakayama K, Watanabe M, et al (2006) Nitroglycerin treatment may enhance chemosensitivity to docetaxel and carboplatin in patients with lung adenocarcinoma. Clin Cancer Res 12:6748-6757

72. Riganti C, Miraglia E, Viarisio D, et al (2005) Nitric oxide reverts the resistance to doxorubicin in human colon cancer cells by inhibiting the drug efflux. Cancer Res 65:516-525

73. Janssens MY, Van den Berge DL, Verovski VN et al (1998) Activation of inducible nitric oxide synthase results in nitric oxide-mediated radiosensitization of hypoxic EMT-6 tumor cells. Cancer Res 58: 5646-5648

74. Yasuda H, Yamaya M, Nakayama K, et al (2006) Randomized phase II trial comparing nitroglycerin plus vinorelbine and cisplatin with vinorelbine and cisplatin alone in previously untreated stage IIIB/IV non-small-cell lung cancer. J Clin Oncol 24:688-694

75. Hagen TL, Eggermont AM (2004) Tumor vascular therapy with TNF: critical review on animal models. Methods Mol Med 98:227-246

76. Blum MS, Toninelli E, Anderson JM, et al (1997) Cytoskeletal rearrangement mediates human microvascular endothelial tight junction modulation by cytokines. Am J Physiol 273:H286-294

77. Romer LH, McLean NV, Yan HC et al (1995) IFN-gamma and TNF-alpha induce redistribution of PECAM-1 (CD31) on human endothelial cells. J Immunol 154:6582-6592

78. Lampugnani MG, Resnati M, Raiteri M, et al (1992) A novel endothelial-specific membrane protein is a marker of cell-cell contacts. J Cell Biol 118:1511-1522

79. Folli S, Pelegrin A, Chalandon Y, et al (1993) Tumor-necrosis factor can enhance radio-antibody uptake in human colon carcinoma xenografts by increasing vascular permeability. Int J Cancer 53:829-836

80. Seki T, Carroll F, Illingworth S et al (2011) Tumour necrosis factor-alpha increases extravasation of virus particles into tumour tissue by activating the Rho A/Rho kinase pathway. J Control Release 156:381-389

81. van Nieuw Amerongen GP, Vermeer MA, Negre-Aminou P et al (2000) Simvastatin improves disturbed endothelial barrier function. Circulation 102:2803-2809

82. de Wilt JH, ten Hagen TL, de Boeck G et al (2000) Tumour necrosis factor alpha increases melphalan concentration in tumour tissue after isolated limb perfusion. Br J Cancer 82:1000-1003

83. van der Veen AH, de Wilt JH, Eggermont AM et al (2000) TNF- α augments intratumoural concentrations of doxorubicin in TNF- α -based isolated limb perfusion in rat sarcoma models and enhances anti-tumour effects. Br J Cancer 82:973-980

84. Roberts AB, Wakefield LM (2003) The two faces of transforming growth factor beta in carcinogenesis. Proc Natl Acad Sci U S A 100:8621-8623

85. Sofuni A, Iijima H, Moriyasu F, et al (2005) Differential diagnosis of pancreatic tumors using ultrasound contrast imaging. J Gastroenterol 40:518-525

86. Takahashi Y, Cleary KR, Mai M et al (1996) Significance of vessel count and vascular endothelial growth factor and its receptor (KDR) in intestinal-type gastric cancer. Clin Cancer Res 2:1679-1684

87. Kano MR, Bae Y, Iwata C et al (2007) Improvement of cancer-targeting therapy, using nanocarriers for intractable solid tumors by inhibition of TGF-beta signaling. Proc Natl Acad Sci U S A 104:3460-3465

88. Minowa T, Kawano K, Kuribayashi H et al (2009) Increase in tumour permeability following TGF- · type I receptor-inhibitor treatment observed by dynamic contrast-enhanced MRI. Br J Cancer 101:1884-1890

89. Kohmoto J, Nakao A, Kaizu T et al (2006) Low-dose carbon monoxide inhalation prevents ischemia/reperfusion injury of transplanted rat lung grafts. Surgery 140:179-185

90. Nakao A, Neto JS, Kanno S et al (2005) Protection against ischemia/reperfusion injury in cardiac and renal transplantation with carbon monoxide, biliverdin and both. Am J Transplant 5:282-291

91. Abraham NG, Kappas A. (2008) Pharmacological and clinical aspects of heme oxygenase. Pharmacol Rev 60:79-127

92. Doi K, Alaike T, Fujii S et al (1999) Induction of haem oxygenase-1 by nitric oxide and ischaemia in experimental solid tumours and implications for tumour growth. Br J Cancer 80:1945-1954

93. Maeda H (2012) Macromolecular therapeutics in cancer treatment: the EPR effect and beyond, J Control Release, in press

94. Maeda H, Matsumura Y, Oda T, Sasamoto K (1986) Cancer selective macromolecular therapeusis; tailoring of an antitumor protein drug. *In*: Feeney RE, Whitaker JR (eds): Protein tailoring for food and medical uses. Marcel Dekker, New York

95. Davis S, Abuchowski A, Park YK, Davis FF (1981) Alteration of the circulating life and antigenic properties of bovine adenosine deaminase in mice by attachment of polyethylene glycol. Clin Exp Immunol 46:649-652

96. Ensor CM, Holtsberg FW, Bomalaski JS, Clark MA (2002) Pegylated arginine deiminase (ADI-SS PEG20,000 mw) inhibits human melanomas and hepatocellular carcinomas in vitro and in vivo. Cancer Res 62:5443-5450

97. Zhao W, Zhuang S Qi XR (2011) Comparative study of the in vitro and in vivo characteristics of cationic and neutral liposomes. Int J Nanomed 6:3087-3098

98. Maeda H, Kimura I, Sasaki Y et al (1992) Toxicity of bilirubin and detoxification by PEG-bilirubin oxidase conjugate: A new tactic for treatment of jaundice. *In*: J. M. Harris (ed): Poly(Ethylene Glycol) Chemistry: Biotech Biomed Applications, Plenum Press, New York, p. 153-169

99. Kimura M, Matsumura Y, Miyauchi Y and Maeda H (1988) A new tactic for the treatment of jaundice: An injectable polymer-conjugated bilirubin oxidase. Proc Soc Exp Biol Med 188: 364-369

100. Li CY, Shan S, Huang Q etal (2000) Initial Stage of Tumor Cell-Induced Angiogenesis: Evaluation Via Skin Window Chambers in Rodent Models. J Natl Cancer Inst 92: 143-147

Figure 1

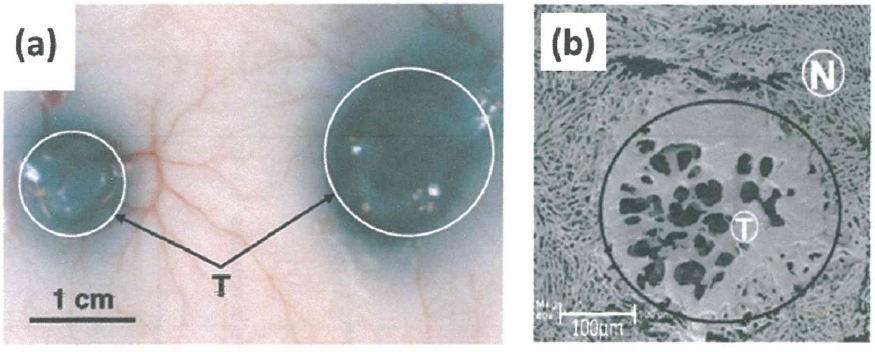

Fig. 1. Illustration of the EPR effect. (a) Tumor-selective accumulation of the putative macromolecular drug Evans blue-albumin complex (MW 67 kDa). The blue color in the macroscopic image indicates macromolecular drug delivery to S-180 tumor implanted in the skin of mice at 24 h after i.v. injection of Evans blue (10 mg/kg). The tumor sites (T, circles, and arrows) show progressive accumulation of Evans blue-albumin, in both small and large tumor. (b) Scanning electron microscopic image of metastatic liver cancer. The tumor (T, circle) is a micrometastatic tumor nodule; even this small nodule shows leakage of a polymer (polyarylate), which is not seen in the surrounding normal tissue (N, in the liver). (Adapted from refs [23]). Dewhirst et al showed that tumor angiogenesis becomes visible when 100-300 tumor cells present [100].

Figure 2.

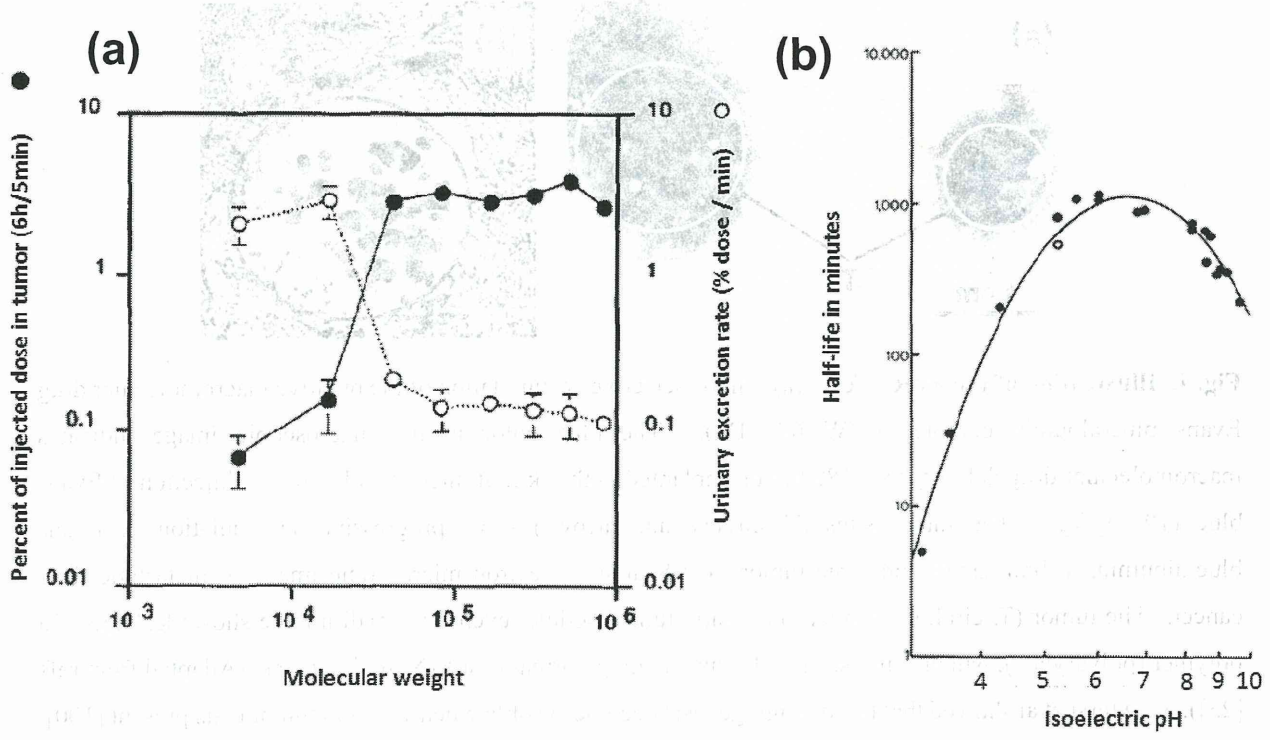

Fig. 2. Influence of the size and charge of macromolecules on their distribution in tumors and plasma concentration. (a) HPMA copolymers, labeled with ^{125}I and of different sizes, were injected i.v. into tumor-bearing mice. The percentage of the injected dose of HPMA in tumor and in urine was calculated. (Adapted from ref [16,23,24]). (b) L-Asparaginase derivatives (MW 120 kDa) with different isoelectric points (pI) after chemical modification were injected i.v. into rabbits (2500 IU/kg), after which the remaining activity of each L-asparaginase derivative was measured and their half-life values in systemic circulation were calculated. (Adapted from ref [39])

Figure 3

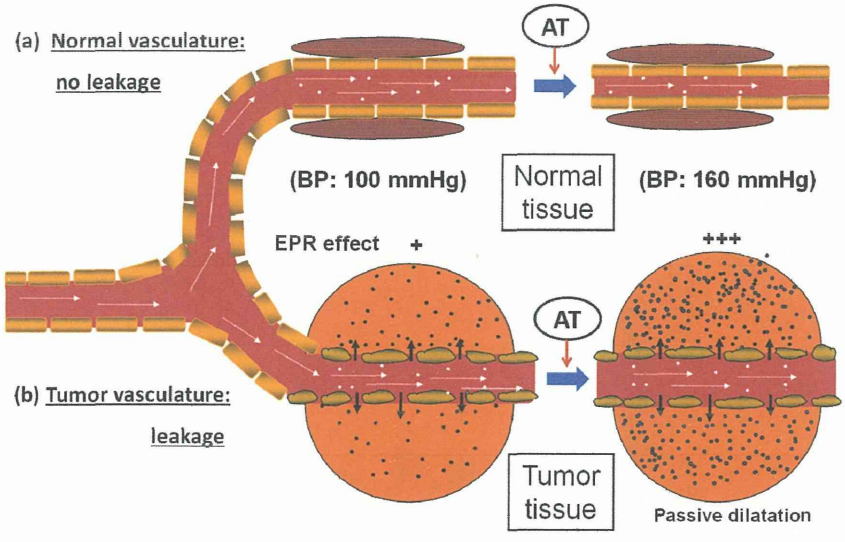

Fig. 3. Diagrammatic representation of the EPR effect and the effect of AT-II-induced enhancement of macromolecular drug delivery to normal and tumor tissue. In the lower part (tumor tissue), angiotensin II (AT-II) infusion induced high blood pressure (e.g., 100 mmHg → 160 mmHg), which caused endothelial cell-cell junctions in the tumor to open and blood flow to increase, with leakage of the macromolecular drug (dark dots). In contrast, normal blood vessels (upper part) constricts in response to AT-II, and tighten the endothelial cell-cell junctions that cause high blood pressure, with no leakage of the drug. AT-II-induced hypertension thus resulted in greater (2–3 fold) leakage of drug into the tumor without increased drug accumulation into normal tissue. (Adapted from ref [24])

Figure 4

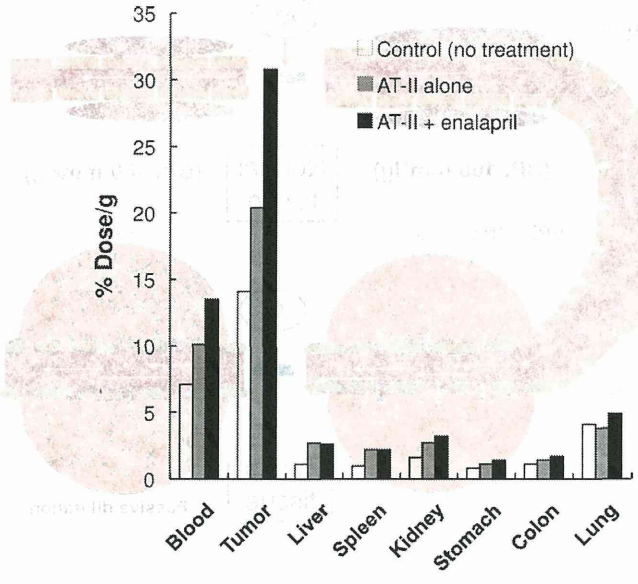

Fig. 4. Augmentation of the EPR effect and delivery of monoclonal antibody to the tumor by using AT-II and the ACE inhibitor enalapril. Human SW11116 colon cancer-bearing nude mice were injected i.v. with ^{125}I-labeled monoclonal antibody A7 with or without AT-II and enalapril. (Adapted from ref [57])

Figure 5

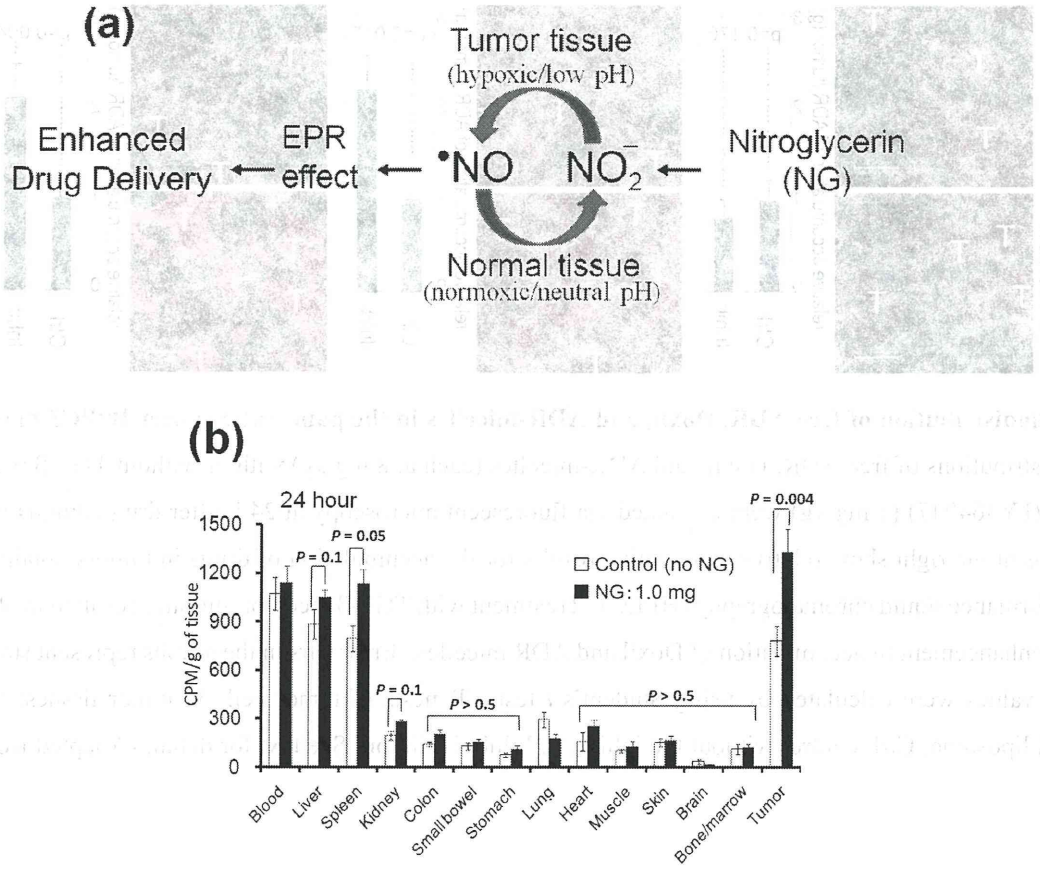

Fig. 5. Nitroglycerin (NG)-induced increase in accumulation of polymer-conjugated drug in tumors. (a) Mechanism of selective NO generation in tumor. NO was generated from nitrite, predominantly in hypoxic tumor tissue, not in normal tissue. (b) In vivo evaluation of the potentiation of drug delivery to tumor by nitroglycerin that was applied as an ointment to anywhere on the skin of S-180 tumor-bearing mice at a dose of 1.0 mg/mouse. Pegylated-^{65}Zn-labeled Zn-protoporphyrin was then injected i.v. into the tumor-bearing mice. After 24 h, anesthetized mice were dissected and radioactivity of each tissue was counted. (Adapted from refs [23,69])

Figure 6

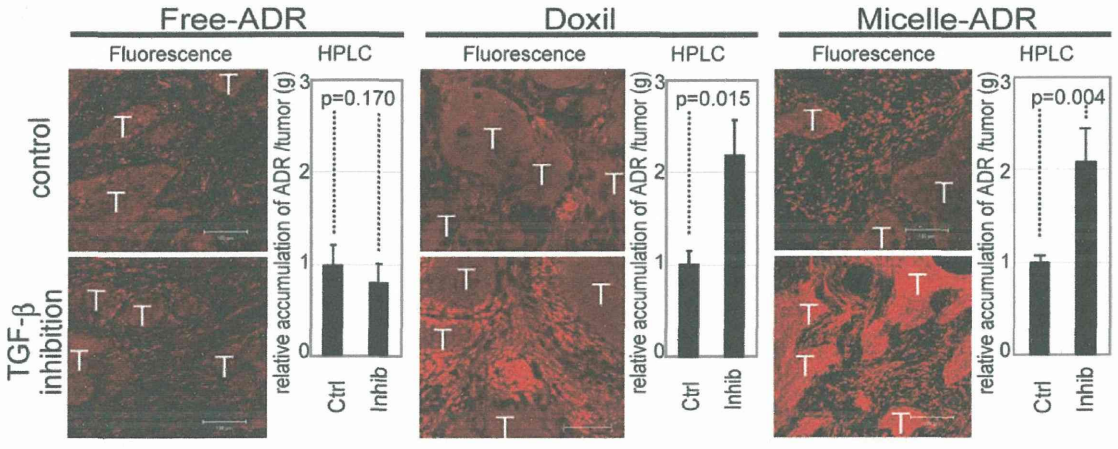

Fig. 6. Biodistribution of free ADR, Doxil, and ADR-micelles in the pancreatic cancer BxPC3 model in mice. Distributions of free ADR, Doxil, and ADR-micelles (each at 8 mg/kg) with or without TGF-β receptor inhibitor (LY364947) (1 mg/kg) were evaluated via fluorescent microscopy at 24 h after drug administration. Bar graphs at the right show relative quantitative results for the accumulation of drugs in tumors obtained by high-performance liquid chromatography (HPLC). Treatment with TGF-β receptor inhibitor resulted in about a two-fold enhancement of accumulation of Doxil and ADR micelles. Error bars in the graphs represent standard errors; *P* values were calculated by using Student's *t* test. T, nests of tumor cells in tumor tissues; Doxil, pegylated liposome; Ctrl, control without the inhibitor; Inhib, inhibitor. See text for detail. (Adapted from ref [87])

Figure 7

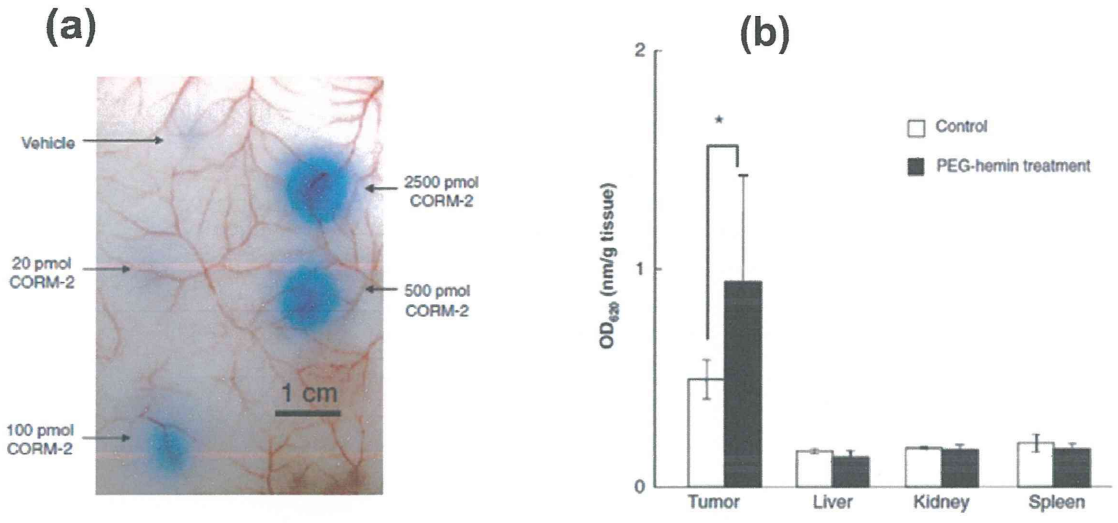

Fig. 7. CO-enhanced accumulation of Evans blue-albumin complex in tumors. (a) Different concentrations of the CO-releasing agent CORM-2 were administered subcutaneously, followed by i.v. injection of Evans blue (10 mg/kg). The dye-albumin complex was allowed to extravasate for 2 h. (b) At 24 h after the i.v. injection of an HO-1 inducer, pegylated hemin (10 mg/kg hemin equivalent), Evans blue was injected as in (a). After another 24 h, mice were killed and dissected to obtain the tissues. Control mice were not treated with pegylated hemin. The blue dye complexed with albumin in each tissue was extracted with formamide, and the degree of extravasation was quantified by means of absorbance at 620 nm. (Adapted from ref [25])

Table 1. Characteristics of the EPR effect of nanomedicine or macromolecular drugs

Biocompatibility	No interaction with blood components or blood vessels, no antigenicity, no clearance by the reticuloendothelial system, no cell lysis
Molecular size	Greater than 40 kDa (larger than the renal clearance threshold)
Surface charge	Weakly negative to near neutral
Time required to achieve	Longer than several hours in systemic circulation in mice
Drug retention time	Mostly days to weeks, in great contrast to passive targeting (in which low-MW molecules are rapidly cleared into the systemic circulation in a few min. cf. low molecular weight contrast agent (see text).

Table 2. Plasma clearance times of selected modified and native proteins in vivo

Protein	Species difference, original/test animal	Probe modification	pI[a]	MW (kDa)	$t_{1/2}$[b]	Note	Ref
• **Albumin**	Mouse/mouse	None	4.8	68	72–96 h	Native, syngeneic	[20,94]
Albumin	Mouse/mouse	DTPA (^{51}Cr)[d]	≦4.8	-	6 h	Slightly surface modified, loss of amino group, syngeneic	
Albumin	Cow/mouse	DTPA (^{51}Cr)[d]	≦4.8	-	1 h	Slightly surface modified, loss of amino group, xenogeneic	
Formaldehyde modified albumin	Human/rat	Formaldehyde ^{125}I	≦4.8	-	25 min	Denatured, loss of amino group, xenogeneic	
• **α_2-Macroglobulin**	Human/mouse	^{125}I	5.3	180×4	140 h	Native, xenogeneic	[20,94]
α_2-Macroglobulin-plasmin complex	Human/mouse	^{125}I	-	180×4	5 min	Inhibitor-protein complex, xenogeneic	
• **Immunoglobulin (IgG)**	Mouse/mouse	DTPA[d]	≦6.8	159	60 h	Slightly surface modified, loss of amino group, syngeneic	[20,94]
• **Interferon α**	Human/human	None		18	8 h (sc)[c]	$t_{1/2}$ 4 min	[20]
Pegylated interferon α2a	Human/human	PEG		52	80 h (sc)[c]		
• **Adenosine deaminase (ADA)**	Cow/mouse	None	4.9	38	<0.5 h	Native, xenogeneic	[95]
Pegylated ADA	Bovine/mouse	PEG[d]	-	>38	28 h, 3–6 days in humans	60% of primary amine conjugated with PEG (5000 Da), xenogeneic	
• **Arginine deiminase (ADI)**	*Mycoplasma hominis*/mouse	Native	5.5	46	<5 h	Native, xenogeneic	[96]
Pegylated ADI	*M. hominis*/mouse	PEG[d]	-	>46	~7 days	10–12 PEG (20,000 Da) attached to each ADI, xenogeneic	
• **Bilirubin oxidase, native[d]**	Microbial/mouse			52	0.25 h		[98,99]
Bilirubin oxidase PEG conjugate	Microbial/mouse			110	5 h		
• **D-amino acid oxidase native**	Pig/mouse			39	14 h		[41]
D-amino acid oxidase PEG conjugate	Pig/mouse			63	36 h		
• **Neocarzinostatin (NCS)**	*Streptomyces*/mouse	DTPA (^{51}Cr)[d]	3.4	12	1.8 min	Slightly surface modified, loss of amino group, xenogeneic	[20,94]
SMA-conjugated NCS (SMANCS)	*Streptomyces*/mouse	DTPA(^{51}Cr)[d], SMA	>3.0	17	19 min	Two chains of SMA (1200 Da) attached to each amino group of NCS; SMA is polyanionic, xenogeneic	

[a]Isoelectric point.
[b]Half-life in systemic circulation (minutes, hours, or days), given i.v. unless otherwise stated.
[c]From microbe, *Myrothecium verrucaria*
[d]DTPA or PEG was reacted with the primary amino group of a lysine residue or N-terminal residue, which made the group much less cationic.
[e]Subcutaneous.

Table 3. Selected parameters affecting plasma residence times of different nanoparticles

Type of nanoparticle	Test animal	ζ potential (mV)	Mean particle size (nm)	Plasma residence time		Remarks	Ref
				$T_{1/2}$	$T_{1/10}$		
· Liposome (nonpegylated)	Mouse	-7.31	124	9.08 h	>24 h	Doxorubicin loaded, DPPC:Chol = 1:1	[97]
Liposome, weakly cationic	Mouse	+5.58	131	4.51 h	15 h (mean)	Doxorubicin loaded, DPPC:Chol:DC-Chol = 5:4:1 slightly positive	
Liposome, strongly cationic	Mouse	+24.25	95	<30 min	<1 h	Doxorubicin loaded, DPPC:DC-Chol = 5:5 strongly positive	
· pLL-DNA complex	Mouse	Positive	-	<5 min	30 min	^{32}P-labeled 8-kbp DNA	[49]
· Chitosan nanoparticle weakly anionic	Mouse	-13.2	149.2	-	12 h (mean)	CMC/MMA = 1:2 slightly negative	[51]
Chitosan nanoparticle strongly anionic	Mouse	-38.4	156.0	-	3 h (mean)	CMC/MMA = 2:1 strongly negative	
Chitosan nanoparticle weakly cationic	Mouse	+14.8	150.1	-	<1 h	CH/MMA = 1:1 slightly positive	
Chitosan nanoparticle strongly cationic	Mouse	+34.6	152.7	-	<1 h	CH/MMA = 2:1 strongly positive	

Abbrebiations: DPPC: L-α-dipalmitoylphosphatidylcholine

Chol: cholesterol

DC-Chol: 3β-[*N*-(*N'*,*N'*-dimethylaminoethyl)carbamoyl]cholesterol

pLL: poly(L-lysine)

CMC: carboxymethyl chitosan

MMA: methyl methacrylate

CH: chitosan hydrochloride

European Journal of Pharmaceutics and Biopharmaceutics 81 (2012) 540–547

Contents lists available at SciVerse ScienceDirect

European Journal of Pharmaceutics and Biopharmaceutics

journal homepage: www.elsevier.com/locate/ejpb

Research paper

HSP32 (HO-1) inhibitor, copoly(styrene-maleic acid)-zinc protoporphyrin IX, a water-soluble micelle as anticancer agent: In vitro and in vivo anticancer effect ☆

Jun Fang [a,b,1], Khaled Greish [a,c,1], Haibo Qin [a,b,d], Long Liao [a,b,d], Hideaki Nakamura [a,b], Motohiro Takeya [e], Hiroshi Maeda [a,b,*]

[a] Laboratory of Microbiology and Oncology, Faculty of Pharmaceutical Sciences, Sojo University, Kumamoto, Japan
[b] DDS Research Institute, Sojo University, Kumamoto, Japan
[c] Department of Pharmacology and Toxicology, University of Otago, Dunedin, New Zealand
[d] Department of Applied Microbial Technology, Sojo University, Kumamoto, Japan
[e] Department of Pathology, Kumamoto University Medical School, Kumamoto, Japan

ARTICLE INFO

Article history:
Received 27 October 2011
Accepted in revised form 21 April 2012
Available online 30 April 2012

Keywords:
HSP32
Heme oxygenase-1
EPR effect
Styrene-maleic acid copolymer
Cancer chemotherapy
Zinc protoporphyrin

ABSTRACT

We reported previously the antitumor effect of heme oxygenase-1 (HO-1) inhibition by zinc protoporphyrin IX (ZnPP). ZnPP per se is poorly water soluble and thus cannot be used as anticancer chemotherapeutic. Subsequently, we developed water-soluble micelles of ZnPP using styrene-maleic acid copolymer (SMA), which encapsulated ZnPP (SMA–ZnPP). In this report, the in vitro and in vivo therapeutic effects of SMA–ZnPP are described. In vitro experiments using 11 cultured tumor cell lines and six normal cell lines revealed a remarkable cytotoxicity of SMA–ZnPP against various tumor cells; average IC_{50} is about 11.1 μM, whereas the IC_{50} to various normal cells is significantly higher, that is, more than 50 μM. In the pharmacokinetic study, we found that SMA–ZnPP predominantly accumulated in the liver tissue after i.v. injection, suggesting its applicability for liver cancer. As expected, a remarkable antitumor effect was achieved in the VX-2 tumor model in the liver of rabbit that is known as one the most difficult tumor models to cure. Antitumor effect was also observed in murine tumor xenograft, that is, B16 melanoma and Meth A fibrosarcoma. Meanwhile, no apparent side effects were found even at the dose of ~7 times higher concentration of therapeutics dose. These findings suggest a potential of SMA–ZnPP as a tool for anticancer therapy toward clinical development, whereas further investigations are warranted.

1. Introduction

Zinc protoporphyrin IX (ZnPP) is a member of metalloporphyrins in which the heme iron is replaced by zinc, which becomes a competitive inhibitor of heme oxygenase (HO). HO is the key enzyme in the degradation of heme and exhibits antioxidative and antiapoptotic effects [1,2]. HO-1 is also a member of heat shock protein (HSP) family, namely HSP32 [2,3]. HO-1 is the inducible isoform of HO as a result of various intracellular and extracelluar stimuli, such as oxystress including superoxide radical, UV irradiation, nitric oxide and hypoxia [2–6]. Subsequently, its critical role in protecting cells against such insults has been reported [2–6].

High expression of HO-1 is now well known in many solid tumors [2,5,6], which is at least partly associated with the hypoxic micro-environment that is common in most solid tumors. Moreover, it is interesting that many cancer cells lost or downregulate antioxidative enzymes such as catalase, superoxide dismutase and glutathione peroxidase [7–11]. HO-1 thus serves as an essential antioxidative and antiapoptotic defense of cancers to support their rapid growth [2,6]. Accordingly, we developed an antitumor strategy by targeting HO-1 in tumors. ZnPP thus became a good candidate for this treatment; however, its poor water-solubility greatly limits its application. To overcome this drawback, we previously developed a water-soluble ZnPP derivative, poly(ethylene glycol)-conjugated ZnPP (PEG–ZnPP), which showed remarkable antitumor effect with very less apparent side effects by selectively targeting tumor based on the EPR (Enhanced permeability and retention) effect [12,13].

Along this line, more recently we developed a micellar type of ZnPP by use of copolymer of styrene-maleic acid (SMA), namely SMA–ZnPP [14]. Similar to PEG–ZnPP, SMA–ZnPP exhibited good

☆ This work was partially supported by a Grant-in-Aid for Research (Nos. 17016076 and 22700927) on Cancer from the Ministry of Education, Culture, Sports and Science of Japan.

* Corresponding author. DDS Research Institute, Sojo University, Ikeda 4-22-1, Kumamoto 860-0082, Japan. Tel.: +81 96 326 4114; fax: +81 96 326 3158.
E-mail address: hirmaeda@ph.sojo-u.ac.jp (H. Maeda).

[1] These authors contributed equally to this paper.

0939-6411/$ - see front matter © 2012 Elsevier B.V. All rights reserved.
http://dx.doi.org/10.1016/j.ejpb.2012.04.016

water solubility, and it remained same HO inhibitory activity compared to native ZnPP. However, the loading of ZnPP in SMA–ZnPP micelle was much higher than that in PEG–ZnPP, which may substantially decrease the net weight of the compounds used for tumor therapy, thus reducing the viscosity of the injection solution and improve the therapeutic effectiveness/cost. Furthermore, from SMA–ZnPP micelle, free ZnPP was released at a constant rate of 20–30%/day. In addition, SMA–ZnPP micelle showed an apparent stoke's radius of 176.5 nm as measured by dynamic light scattering in a physiological solution [14]. It will further show a larger molecular size in circulation because of the albumin binding property of SMA [15,16]. Thus, the sustained in vivo antitumor effect was anticipated.

To investigate the therapeutic potential of SMA–ZnPP, in this study various tumor strains and normal cell lines were used to examine the pharmacological activity of SMA–ZnPP and the in vivo antitumor effect was evaluated by using various murine and rabbit tumor models. The intracellular uptake, pharmacokinetics and body distribution of SMA–ZnPP, and the safety were also investigated.

Table 1
IC_{50} of SMA–ZnPP against various tumor cells and normal cells.

Tumor cells	IC_{50} (μM)	Normal cells	IC_{50} (μM)
DLD-1	14.0	CV-1	50.0
Sk-Hep	16.0	HBE140	>50.0
HT-29	5.8	RLF	>200.0
A431	15.0	Hc	>50.0
KP-1N	3.6	HEK293	>50.0
CNE	19.4	CEF	25.2
ES2	9.8		
Lxc	4.2		
MCF-7	3.1		
Meth A	10.8		
B16/F10	20.1		
Mean	11.1 ± 1.9	Mean	>50.0

IC_{50} was determined by the MTT assay. See text for details.
DLD-1 and HT-29, human colon cancer cells; Sk-Hep, human liver cancer cell; A431, human lung cancer cell; CNE and Lxc, human laryngeal cancer cells; ES2, human ovarian cancer cell; KP-1N, human pancreatic cancer cell; MCF-7, human breast cancer cell; Meth A, mouse fibrosarcoma cell; B16/F10, mouse melanoma cell. CV1, monkey kidney fibroblast; HBE140, human bronchial epithelial cell; RLF, rat liver fibroblast; HEK293, human embryonic kidney cell; CEF, chick embryonic fibroblast; Hc, human hepatic cell.

2. Materials and methods

2.1. Materials

Protoporphrin IX was purchased from Sigma-Aldrich (St. Louis, MO). SMA with a mean molecular size of 1280 Da (Mw/Mn: 1.1) was obtained from Kuraray Ltd., Kurashiki, Japan. Other reagents were of commercial reagent grade and were used without further purification.

2.2. Animals

Female BALB/c mice and male C57BL/6 mice, 5–6 weeks of age and weighing 20–25 g, as well as New Zealand white rabbits about 3 months old, weighing 2.0–2.25 Kg, were from SLC, Inc. (Shizuoka, Japan). All experiments were carried out according to the guidelines of the Laboratory Protocol of Animal Handling, Sojo University.

2.3. Synthesis of SMA–ZnPP micelles

The preparation, purification and characterization of SMA–ZnPP micelle were described in our recent work [14].

2.4. In vitro cytotoxicity assay

In vitro cytotoxicity of SMA–ZnPP micelles was examined by use of MTT assay with 11 tumor cell lines and six normal cell lines as described in Table 1. Cells were plated in 96-well culture plates (3000 cells/well). After overnight pre-incubation, predetermined concentration of SMA–ZnPP was added to respective culture media, and the cells were further incubated for 72 h. Toxicity was quantified as the fraction of surviving cells relative to untreated controls.

2.5. Intracellular uptake of SMA–ZnPP

Intracellular uptake study was carried out in human laryngeal cancer cells Lxc. 50,000 cells were cultured in 16-well plates. After 12 h of culture, SMA–ZnPP solution in deionized water or free ZnPP, dissolved first in DMSO and then diluted with 0.01 M NaOH, were added to the cells at dose of 5 μM ZnPP equivalent. The medium containing drug was removed at predetermined time, and the cells were washed twice with PBS. Cells were then lysed by 1 ml lysis buffer (4 N HCl in 70% ethanol) then heated to 70 °C for 15 min. The solution was centrifuged at 15,000 rpm for 3 min, and the supernatant was used for measuring the fluorescence emission from 550 to 600 nm by excitation at 420 nm (corresponding to ZnPP) using a fluorescence spectroscopy (Hitachi F-4500, Tokyo, Japan). Experiments were also carried out in mouse fibrosarcoma Meth A cells and mouse melanoma B16/F10 cells similarly.

2.6. Pharmacokinetics of SMA–ZnPP after i.v. injection into tumor-bearing mice

In vivo pharmacokinetics of SMA–ZnPP was examined by the use of ^{65}Zn-radiolabeled derivatives. Radiolabeled SMA–ZnPP was prepared by the same method as that described by Iyer et al [14], in which ^{65}Zn-labeled zinc acetate (Riken, Saitama, Japan) was used.

Mouse sarcoma S180 cells (2×10^6) were implanted, s.c. in the dorsal skin of ddY mice. At 10–15 days after tumor inoculation when tumors reached a diameter of 7–10 mm, each mouse received i.v. injections of ^{65}Zn-labeled SMA–ZnPP via the tail vein [50 μg ZnPP equivalent, 45,000 cpm (0.75 kBq), 0.2 ml/injection]. After scheduled time, mice were killed, blood samples were drawn from the inferior vena cava, and mice were then subjected to reperfusion with 20 ml of physiological saline containing heparin (5 units/ml) to remove blood components in the blood vessels of the tissues. Then, tumor tissues as well as normal tissues, including the liver, the spleen, the kidney, the intestine, the heart, the lung, the brain and the muscle, were collected and weighed. Radioactivity of these tissues was measured by using a gamma counter (1480 WIZARD, Perkin Elmer, Waltham, MA).

The pharmacokinetics of SMA–ZnPP was also examined in Meth A and B16 tumor-bearing mice as described below, by measuring the fluorescence intensity at 590 nm of ZnPP. Namely, at schedule time after SMA–ZnPP (20 mg/kg, ZnPP equivalent) i.v. injection, mice were killed and each tissue and organ was resected. Each tissue was then weighted, and dimethylsulfoxide was added at a ratio of 1 mL/100 mg tissue, followed by homogenization to extract the SMA–ZnPP by centrifugation (12,000 g, 25 °C, 10 min) to precipitate the insoluble tissue debris. Content of SMA–ZnPP in the supernatant was quantified by fluorescent intensity (Ex. 422 nm, Em. 590 nm).

2.7. In vivo antitumor effect of SMA–ZnPP

Mouse Meth A fibrosarcoma and melanoma B16 were prepared by implanting Meth A and B16/F10 cells (2×10^6 cells) s.c. in the dorsal skin of BALB/c and C57BL/6 mice, respectively. On day 7–10 after tumor injection when tumors had reached a diameter of 5–7 mm, SMA–ZnPP micelles at the desired concentration were administered intravenously via the tail vein according to the treatment protocol. Growth of the tumors was monitored every 2 days by measuring tumor volume with a digital caliper, which was estimated by measuring longitudinal cross section (L) and transverse section (W) according to the formula $V = (L \times W^2)/2$.

VX-2 carcinoma that is a papilloma virus–induced squamous cell carcinoma was established in New Zealand white rabbits. Briefly, laparotomy was performed with central incision, using pentobarbital sodium for general anesthesia at dose of 30 mg/kg intravenously. A solid VX-2 tumor mass of about $2 \times 2 \times 2$ mm^3 was inoculated through forceps into the subcapsular parenchyma of left anterior lobe of the liver. Fourteen days after tumor inoculation, intravenous treatment with SMA–ZnPP (once a week) was commenced for successive 4 weeks. One month after treatment, another laparotomy was performed and the liver was exposed to measure the diameter of tumor. Three months after tumor inoculation, all survived animals were sacrificed, and liver biopsy from the tumor site was collected for histological examination.

2.8. Histological examination

Tissue specimens collected from VX-2 tumor models as described above were fixed with 10% buffered neutral formalin solution and were then embedded in paraffin. Sections were stained with H&E as usual.

2.9. Measurement of HO activity

Meth A, B16 and S180 tumor tissues, collected from tumor-bearing mice after 24 h with or without i.v. injection of SMA–ZnPP (20 mg/kg, ZnPP equivalent), were homogenized by a Polytron homogenization with ice-cold homogenate buffer [20 mM potassium phosphate buffer (pH 7.4) plus 250 mM sucrose, 2 mM EDTA, 2 mM phenylmethylsulfonyl fluoride, and 10 μg/ml leupeptin]. Homogenates were centrifuged at 10,000g for 30 min at 4 °C, after which the resultant supernatant was ultracentrifuged at 105,000g for 1 h at 4 °C. The microsomal fraction was suspended in 0.1 M potassium phosphate buffer (pH 7.4) followed by sonication for 2 s at 4 °C. The reaction mixture used for measuring HO activity composed of microsomal protein (1 mg), cytosolic fraction of rat liver (1 mg of protein) as a source of biliverdin reductase, 33 μM hemin and 333 μM NADPH in 1 ml of 90 mM potassium phosphate buffer (pH 7.4). The mixture was incubated for 15 min at 37 °C, and then, the reaction was terminated by the addition of 33 μl of 0.01 M HCl. The bilirubin formed in the reaction was extracted with 1 ml of chloroform, and the bilirubin concentration was determined spectrophotometrically by measuring the difference in absorbance between 465 and 530 nm, with a molar extinction coefficient of 40 mM^{-1} cm^{-1}.

2.10. Safety of SMA–ZnPP micelles

BALB/c mice with Meth A tumors of about 5–7 mm in diameter were used for this study. SMA–ZnPP micelles were administered at the dose of 50 mg/kg (ZnPP equivalent), which is 5–10 times higher concentration than therapeutic dose. Seventy-two hours later, mice were killed and blood samples were obtained. RBC, WBC counts and hemoglobin levels were determined by using an automated blood counter (F-800 Microcell Counter, Toa Medical Electronics, Kobe, Japan). Plasma obtained by centrifugation was used for measurement of enzyme activities of alanine aminotransferase, aspartate aminotransferase, lactate dehydrogenase, blood urea nitrogen and total creatine values by using a sequential multiple Auto Analyzer system (Hitachi Ltd., Tokyo, Japan).

2.11. Statistical analyses

All data were expressed as means ± SD. Student's t-test was used to compare differences between experimental groups, and it was considered statistically significant when $p < 0.05$.

3. Results

3.1. In vitro cytotoxicity of SMA–ZnPP

In human liver cancer Sk-Hep cells, SMA–ZnPP exhibited remarkable cytotoxicity, in a dose-dependent manner, whereas

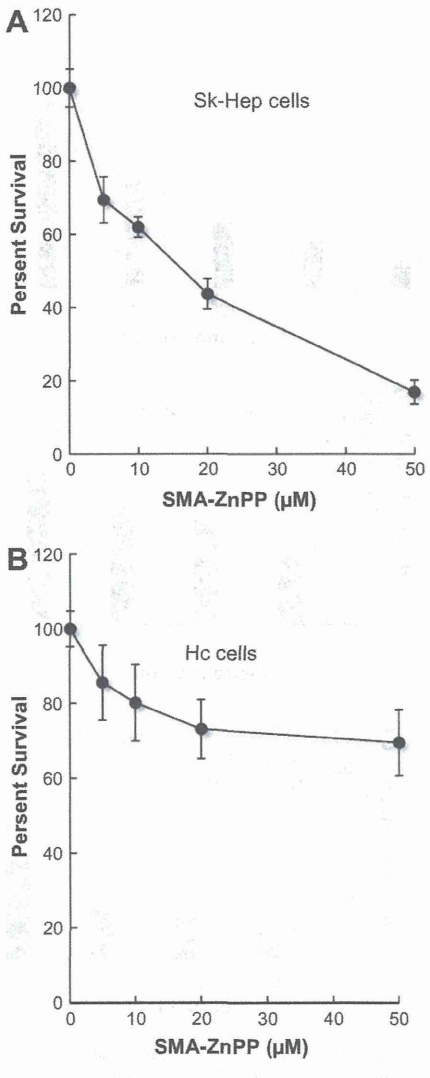

Fig. 1. In vitro cytotoxicity of SMA–ZnPP against normal (Hc) and tumor (Sk-Hep) cells. Cells were exposed to increasing concentration of SMA–ZnPP for 48 h, followed by MTT assay to determine cell viability. Values are mean ± SE (n = 6–8).

no significant cytotoxicity was observed up to 50 μM against normal hepatocytes Hc (Fig. 1 and Table 1). Similar results were found in other tumor and normal cell lines. The average 50% inhibitory concentration (IC_{50}) of SMA–ZnPP against different cells was summarized in Table 1. Most normal cells tested in this study exhibited relative tolerance to SMA–ZnPP treatment with IC_{50} of higher than 50 μM. In contrast, tumor cells showed much sensitive to this treatment, whose average IC_{50} was 11.1 ± 1.9 μM.

3.2. Intracellular uptake of SMA–ZnPP micelle

Fig. 2A shows a time-dependent internalization of SMA–ZnPP into Lxc cells, which is comparable to that of free ZnPP. These results suggest that the micellar formation of SMA did not impede the intracellular uptake of SMA–ZnPP. Instead, SMA–ZnPP appears more favorable than PEG–ZnPP micelles whose internalization was about 1/3 of that of SMA–ZnPP at 6 h after addition to the culture media (Fig. 2A). Similar results were obtained in Meth A (Fig. 2B) and B16/F10 cells (Fig 2C).

3.3. Pharmacokinetics and body distribution of SMA–ZnPP after i.v. injection

As shown in Fig. 3A, no significant prolonged plasma half-life ($t_{1/2}$) was observed for SMA–ZnPP. Namely, more than 50% of the SMA–ZnPP was removed from circulation during 10 min after i.v. injection. Moreover, no significant tumor accumulation of SMA–ZnPP was achieved, for example, the tumor concentration of SMA–ZnPP at 24 h after SMA–ZnPP administration was similar to those of most normal tissues (Fig. 3B).

However, surprisingly we found a remarkable increase in liver delivery of SMA–ZnPP, which is more than 20 times of that in plasma at 24 h after i.v. injection (Fig. 3A). Accumulation of SMA–ZnPP in liver tissue remained high for at least 4 days (Fig. 3A). Similar results were also observed in Meth A fibrosarcoma tumor and B16 melanoma tumor-bearing mice, respectively (Fig. S1). These findings suggested the potential application of SMA–ZnPP for cancers in the liver.

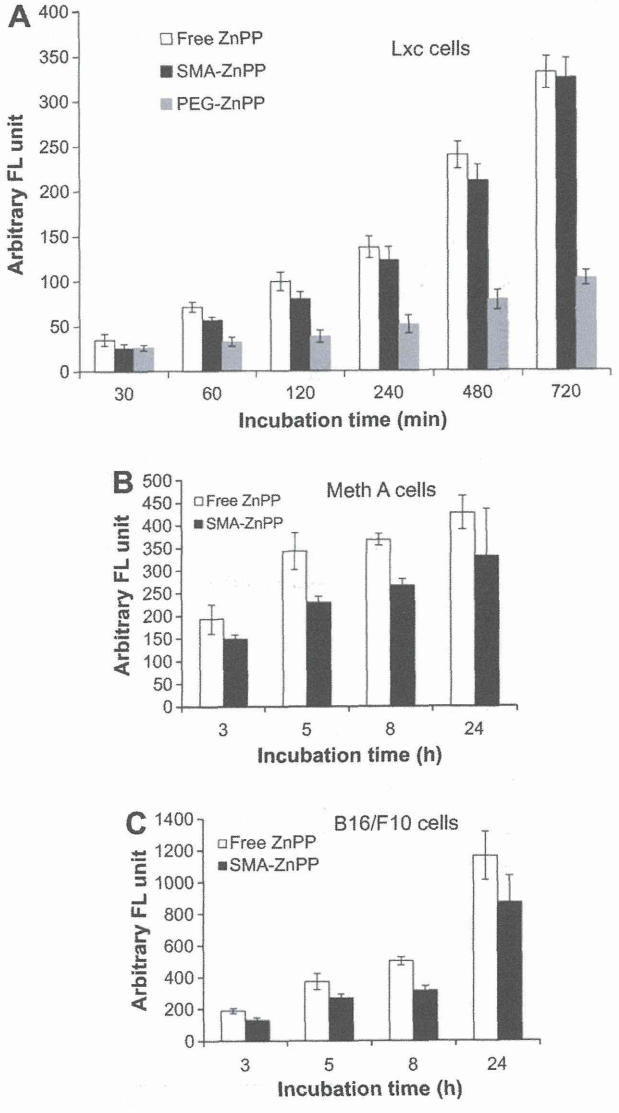

Fig. 2. Intracellular uptake of free ZnPP, SMA–ZnPP and PEG–ZnPP. Lxc cells (A), Meth A cells (B) and B16/F10 cells (C) were incubated with the investigated compounds at 5 μM (expressed in ZnPP equivalents) for different period of time. The amount of drug uptake by different tumor cells was determined measuring the fluorescence intensity after extracted from the cells, as described in Materials and Methods (2.5.). Values are mean ± SE ($n = 4$).

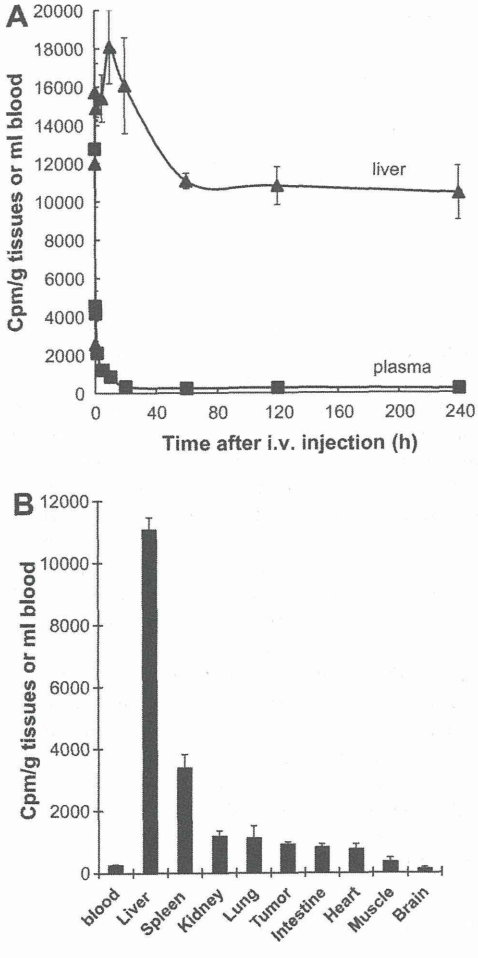

Fig. 3. Pharmacokinetics of SMA–ZnPP in ddY mice bearing Sarcoma 180 tumor as determined by using radioactive derivatives. Radiolabeled SMA–ZnPP was injected i.v. into tumor-bearing mice. After scheduled time periods, mice were killed, and samples of blood, tumor, liver and other normal tissues and organs were collected. Radioactivity of each tissue or organ was then measured. *A*, time-dependent change in SMA–ZnPP concentrations in plasma (■) and liver (▲). *B*, body distribution of SMA–ZnPP at 24 h after i.v. injection. Data are expressed as means; bars, ±SE ($n = 4$).